Electrode-Based Dielectrophoretic Separation of Live and Dead Yeast Cells

Shiriny, Afshin;Bayareh, Morteza*+; Ahmadi Nadooshan, Afshin
Department of Mechanical Engineering, Shahrekord University, Shahrekord, I. R. IRAN

ABSTRACT: *This paper investigates the electrode-based dielectrophoretic (eDEP) separation of live and dead yeast cells with diameters of 6 and 5 μm using COMSOL Multiphysics 5.6 software. Five electrodes are placed on one side of a rectangular microchannel with three inlets and three outlets. A non-uniform electric field is created inside the microchannel by applying an alternating electric field (AC) to the electrodes. Microchannel inlets include an inlet for injecting a sample fluid consisting of deionized water containing two species of live and dead yeast cells and two inlets for injecting deionized water as a sheath flow to concentrate the cells before reaching the area affected by the electric field. The study is conducted in two dimensions and the effect of various factors, including the electrical voltage applied to the electrodes (V_e), the frequency (f), the length of the electrodes, their distance from each other, and the inlet velocity on the efficiency and purity of cell separation is examined. In addition, the optimal conditions for achieving complete separation of live and dead yeast cells utilizing the proposed microfluidic device are presented as follows: u_{Sample} = 60 μm/s, u_{Buffer} = 360 μm/s, V_e = ±4.35 V, and f = 3.18 MHz.*

KEYWORDS: *Microfluidic device; Cell separation; Dielectrophoresis; Yeast cells; Purity.*

INTRODUCTION

Cell isolation is a pivotal step in biological research that is used in many fields, including medicine, pharmacy, food production, and environmental monitoring. Isolation of live and dead cells is critical to detect the early stages of the disease and to test the effectiveness of drug screening [1]. Conventional methods of separating live and dead cells, including centrifugation, chromatography, and fluorescence, have low separation efficiencies and purity and also require the employment of highly specialized personnel [2]. In recent years, the advent of microfluidic technology due to its unique features including the need for low sample consumption, portability, high efficiency, cost reduction, high sensitivity, and rapid detection has led to cell isolation by using these devices. Different types of microfluidic cell separation methods include active techniques using an external field such as electric, acoustic, optical, magnetic field, and passive ones without employing an external field including hydrodynamic separation, microfiltration, inertial, and Deterministic Lateral Determination (DLD) [3, 4]. Existing methods often require cell labeling for detection and isolation. Labeling is done by using magnetic bonding or fluorescence of external labels to the target cells. Among these, the use of a non-uniform electric field or DEP is one of the methods of separating live and dead cells without cell labeling [1]. In this method, the isolation process is based on the intrinsic

*** To whom correspondence should be addressed.*
+ E-mail: m.bayareh@sku.ac.ir
1021-9986/2023/6/1796-1810 15/$/6.05

and dielectric properties of cells. Therefore, as a non-invasive and non-destructive method, concerns about cell viability and alteration of their function are eliminated. When a cell is exposed to a non-uniform electric field, positive and negative charges accumulate on the interface between the cell and its suspension. Because the electric field causes the electric charges to be transferred toward the opposite direction, an effective dipole moment is induced in the cell. In this case, the cell is polarized, i.e. it is oriented in the direction of electric field vectors [5, 6]. Isolation of live and dead cells is based on DEP: when the cells move towards the area with high electric field strength, i.e. positive dielectrophoresis (pDEP), or when they move towards the area with low electric field intensity, i.e. negative electrophoresis (nDEP). The polarization of a cell depends on the electrical properties of the cell, including electrical conductivity and electrical permittivity, and the mechanical properties of the cell such as cell size and shape as well as the frequency of the electric field. It has been reported that if cells lose their viability, their electrical conductivity decreases at the cell nucleus and increases at the cell membrane [6]. Therefore, the response of live and dead cells to electric fields, especially AC electric fields and fields with an electric frequency higher than 100 kHz, can be different [1]. One of the most widely used methods of DEP is the use of a non-uniform AC electric field and an array of electrodes inside the microchip. Two-dimensional (flat) electrodes are placed on the upper and lower walls of the microchannel and three-dimensional electrodes are placed on the sidewalls of the microchannel. Different types of rectangular, trapezoidal, curved, and spiral electrodes have been used in eDEP in various studies [7, 8]. Under a suitable electric field, live cells are absorbed by pDEP with higher electric field strength, and dead cells move away to a region with lower electric field strength [1].

The eDEP has been the subject of extensive studies performed experimentally, numerically, or a combination of both methods. Using DEP, *Xing et al.* [9] isolated intestinal cancer cells from white blood cells with efficiencies of 82% and 99%, respectively. In this study, a field with frequency $f = 100\,\text{kHz}$ and voltage of $V_{PP} = 10\,V$ was utilized. In an experimental study, *Pommer et al*. [10] employed a two-stage microfluidic device to isolate blood platelets from red blood cells using DEP. The frequency and voltage of their applied field were reported to be 1 MHz and 100 V, respectively. *Yang et al.* [11] isolated colorectal cancer cells (HCT116) from intestinal bacteria (E. coli) and human renal embryonic cells (HEK293) by using the DEP method. They inserted two triangular flat electrodes into the channel and applied a voltage of 1.5 V and a frequency of 100 Hz to achieve a separation efficiency of 98%. *Nie et al.* [12] also used DEP to separate the live and dead Hele cells by applying a voltage of 17.5 V and a frequency of 400 kHz with a purity of 99.1% and 92.8%, respectively.

In the field of numerical modeling of microfluidic separation, one of the most powerful software is COMSOL Multiphysics software due to the accurate prediction of particles/cells motion and modeling of multi-physical studies [13-15]. *Kumar et al*. [16] employed this software to isolate E.coil bacteria with a diameter of 0.68 μm from platelets and red blood cells with diameters of 1.8 and 5 μm, respectively. Their proposed microchannel consisted of 7 electrodes located on the sidewall of the channel with two inlets and two outlets. They reported the appropriate voltage and frequency of ±19.5 V and 100 kHz, respectively, for complete isolation of the mentioned cell species. *Kumar et al.* [17] completely separated red, white, and platelet cells with diameters of 5, 9.4, and 1.8 μm with a voltage of 1.5 V and a frequency of 100 kHz. They designed one of the sidewalls of the microchannel in a zigzag pattern and placed the positive and negative electrodes on the zigzag ones. *Guan et al.* [18] separated 1.8-μm platelets from 5-μm red blood cells using DEP force. Their proposed microchannel has a zigzag pattern consisting of two inlets and two outlets. They reported complete separation for a voltage of ±20 V, a frequency of 10^{-3} Hz, and a zigzag angle of 120°. *Piacentini et al.* [19] modeled the complete separation of platelets from red blood cells experimentally and numerically using seven positive and negative electrodes placed on the sidewalls of the microchannel when a voltage of 5 V was applied. *Caffiyar et al.* [20] simulated the separation of white and red blood cells and platelets and proposed a microchannel consisting of two inlets and three outlets and an array of triangular electrodes laced on a part of the sidewall. A positive voltage was applied to the electrodes and a negative voltage was applied to the wall in front of the electrodes. Optimal conditions for complete isolation of the three cell types were reported as a frequency of 110 kHz, a voltage of 9 V, and sample and buffer flow rates of 150 μm/s and 700 μm/s, respectively.

To the best of the authors' knowledge, few researchers have examined the separation of live and dead cells experimentally and numerically. For the numerical example, *Doh et al.* [21] used a rectangular microchannel consisting of three inlets and three outlets to separate live and dead saccharomyces cerevisiae yeast cells with a diameter of 6 and 5 μm, respectively. They utilized dielectrophoretic force caused by a flat electrode mounted on the bottom wall of a microchannel. Live and dead yeast cells were isolated with an efficiency of 97.3-95.9% and 74.3-64.5%, respectively, by applying $V_{PP} = 8$ V and $f = 5$ MHz. Experimental investigations are also limited to a few works. For instance, *Patel et al.* [1] employed reservoir-based electrophoresis (rDEP) to perform their experiments. Besides, a complementary metal-oxide-semiconductor (CMOS) channel was used by *Matbaechi Ettehad* and *Wenger* [22] and *Park et al.* [23] to separate yeast cells using DEP microfluidics.

In this study, for the first one, the isolation of live and dead yeast cells is performed using the eDEP technique numerically. The effect of various parameters such as the voltage applied to the electrodes, length of the electrodes, the distance between the electrodes, inlet velocity, and frequency on the separation rate of live and dead yeast cells are evaluated. The proposed microfluidic device can be utilized for practical applications such as food sciences.

THEORY AND GOVERNING EQUATIONS

The physics of the problem under study consists of three general parts: Fluid flow, electric field, and particle motion. In the fluid flow section, the main equations governing the problem are continuity and momentum (Navier-Stokes) equations. Due to the small amount of fluid velocity and also the proposed microchannel dimensions, the Reynolds number is in the range of the creep flow regime (Re < 1); thus, the continuity and Navier-Stokes equations for incompressible and steady fluid flow are expressed as follows:

$$\nabla \cdot \mathbf{u} = 0 \tag{1}$$

$$-\mu\nabla^2\mathbf{u} + \nabla p = 0 \tag{2}$$

where $\mathbf{u}$ is the fluid velocity vector, p is the pressure, and μ is the dynamic viscosity of the fluid.

The electric current regime consists of the generalized Ohm's law and Gauss law and the electric current conservation equation [3]:

$$\mathbf{E} = -\nabla \cdot \mathbf{V} \tag{3}$$

$$\nabla \cdot [(\sigma_m + j\omega\varepsilon_0\varepsilon_m)\nabla\mathbf{V}] = 0 \tag{4}$$

Here, $\mathbf{E}$ and $\mathbf{V}$ are the electric field strength and the electric potential, respectively. Also, $j = \sqrt{-1}$ and σ_m and ε_m represent the electrical conductivity coefficient and the relative electrical permittivity of the fluid, respectively. $\varepsilon_0 = 8.548 \times 10^{-10}$ F/m is the electrical permittivity of a vacuum. In addition, $\omega = 2\pi f$ is the angular frequency and f is the frequency of the electric current.

Particle motion is modeled using Newton's second law by applying DEP forces and hydrodynamic drag as follows:

$$\frac{d}{dt}(mv)\left[F_{drag}\right] + F_{DEP} \tag{5}$$

where m and $\mathbf{v}$ are the mass and velocity of cells, respectively. $\mathbf{F}_{drag}$ is the hydrodynamic drag force calculated as follows:

$$\mathbf{F}_{drag} = 6\pi\mu a(\mathbf{u} - \mathbf{v}) \tag{6}$$

$\mathbf{F}_{DEP}$ is also the DEP force [3]:

$$\mathbf{F}_{DEP} = 2\pi\varepsilon_0\varepsilon_m a^3 \mathrm{Real}[K(\omega)]\nabla|\mathbf{E}|^2 \tag{7}$$

Here, $K(\omega)$ is the polarization factor that is defined as follows:

$$CM = \frac{\varepsilon_c^* - \varepsilon_m^*}{\varepsilon_c^* + 2\varepsilon_m^*} \tag{8}$$

where ε_c^* and ε_m^* are the mixed electrical permittivity of the particle and the medium, respectively:

$$\varepsilon^* = \varepsilon_0\varepsilon - j\left(\frac{\sigma}{\omega}\right) \tag{9}$$

Where ε and σ are the relative permittivity coefficient and electrical conductivity of the fluid or cell, respectively. To calculate the cell permittivity coefficient, the multi (double)-shell model is employed, which is suitable for the cell consisting of a shell and core with different electrical conductivity. In this model, a smaller sphere (cell nucleus) with a shell (membrane) is placed inside a larger sphere as shown in Fig. 1. Thus, ε_c^* can be calculated using the following equations [24]:

$$\varepsilon_c^* = \varepsilon_w^* \frac{\left(\frac{a}{a_m}\right)^3 + 2\left(\frac{\varepsilon_{mn}^* - \varepsilon_w^*}{\varepsilon_{mn}^* + 2\varepsilon_w^*}\right)}{\left(\frac{a}{a_m}\right)^3 - \left(\frac{\varepsilon_{mn}^* - \varepsilon_w^*}{\varepsilon_{mn}^* + 2\varepsilon_w^*}\right)} \tag{10}$$

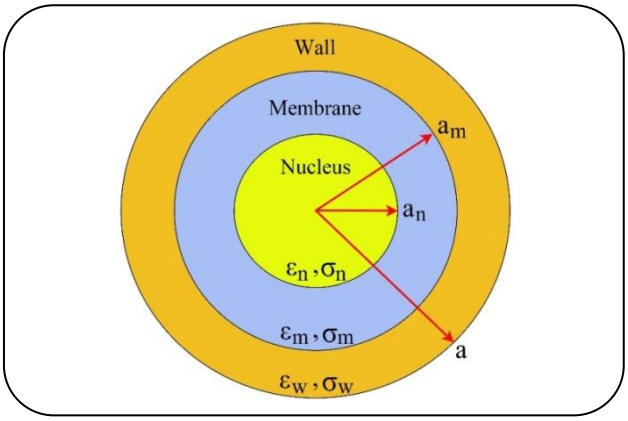

Fig. 1: Double-shell model of a yeast cell.

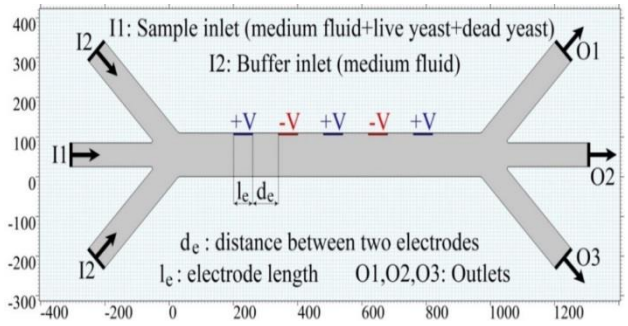

Fig. 2: Proposed microchannel geometry (dimensions in micrometers).

$$\varepsilon_{mn}^{*} = \varepsilon_{m}^{*} \frac{\left(\frac{a_m}{a_n}\right)^3 + 2\left(\frac{\varepsilon_n^{*} - \varepsilon_m^{*}}{\varepsilon_n^{*} + 2\varepsilon_m^{*}}\right)}{\left(\frac{a_m}{a_n}\right)^3 - \left(\frac{\varepsilon_n^{*} - \varepsilon_m^{*}}{\varepsilon_n^{*} + 2\varepsilon_m^{*}}\right)} \qquad (11)$$

It should be noted that ε_n^*, ε_m^* and ε_w^* are the mixed permittivity coefficients of the nucleus, membrane, and cell wall, respectively. They can be calculated using Eq. (9) when the values of ε and σ are presented in Table 1. Also, a_n and a_m are the radii of the cell nucleus and membrane, respectively. If t_w and t_m are the thicknesses of the cell membrane and wall, respectively, a_n and a_m can be calculated using the following equation:

$$a_m = a - t_w \qquad a_n = a_m - t_m \qquad (12)$$

NUMERICAL METHOD

The proposed microdevice is shown in Fig. 2. The flow containing live and dead yeasts with diameters of 6 and 5 μm, respectively, is injected into the microchannel from the middle inlet I1. A stream consisting of a suspension medium of yeast cells (without the presence of yeasts) called a buffer or sheath flow enters the microchannel from inlets I2 and I3 to concentrate the yeasts on the centerline of the main microchannel. Three electrodes with positive voltage and two electrodes with negative voltage are placed on one sidewall of the microchannel. The length of electrodes is l_e and their distance is d_e. The length and width of the main channel are equal to 1000 and 110 μm, respectively. The inlets and outlets are located at an angle of 45° relative to the middle inlet and outlet. The width of the side inlets and outlets is 70 μm and the width of the middle ones is 60 μm. The suspension fluid is deionized water. The physical properties of the fluid and cells used in this study are presented in Table 1.

The fluid flow is first solved as a single phase (continuous phase) using the Eulerian approach by employing the PARDISO solver. The inlet velocity boundary condition is used for inlets, the non-slip boundary condition is imposed on the microchannel walls and pressure output one is employed for outlets to model the continuous incompressible fluid flow. As shown in Fig. 2, positive and negative voltages are applied to the electrodes, and microchannel walls are considered as electrical insulation. The physics of electric current is permanently solved using the second frequency which is suitable for modeling the AC field with the help of the MUMPS solver. Then, the Lagrangian approach is used to model the motion of cells (discrete phase). The fluid velocity field solution is used as velocity input to predict the motion of yeast cells. The equations governing the physics of cell motion are solved by the GMRES solver. Table 2 presents the various parameters considered for the simulations.

VALIDATION

To ensure the accuracy of the numerical method, the present results are compared with the experimental data of *Piacentini et al.* [19], who separated white blood cells and platelets suspended in the phosphate-buffered saline (PBS) suspension using DEP force due to the placement of 7 electrodes on the sidewall of the microchannel. Particulate flow and buffer flow velocities are 134 μm/s and 853 μm/s, respectively. Also, an electrical potential of 5 V is applied to each electrode. The diameter of platelets and red blood cells is 1.8 μm and 5 μm, respectively, and the applied frequency is set to 100 kHz. Figs. 3A and 3B show the

Table 1. Physical properties of fluid and cells [1].

Parameter	Value
Density of medium fluid, ρ	1000 kg/m³
Dynamic viscosity of the medium fluid, μ	0.001 Pa.s
Electrical conductivity of the medium fluid, σ_m	0.021 S/m
Relative permittivity of medium fluid, ε_m	78
Diameter of live yeast, a_l	6 μm
Diameter of dead yeast, a_d	5 μm
Density of live yeast, ρ_l	1110 kg/m^3
Density of dead yeast, ρ_d	1110 kg/m^3
Nucleus relative permittivity of live yeast, ε_{nl}	50
Nucleus relative permittivity of dead yeast, ε_{nd}	50
Nucleus electrical conductivity of live yeast, σ_{nl}	0.2 S/m
Nucleus electrical conductivity of dead yeast, σ_{nd}	0.007 S/m
Membrane relative permittivity of live yeast, ε_{ml}	6
Membrane relative permittivity of dead yeast, ε_{md}	6
Membrane electrical conductivity of live yeast, σ_{ml}	0.25 μS/m
Membrane electrical conductivity of dead yeast, σ_{md}	0.16 mS/m
Wall relative permittivity of live yeast, ε_{wl}	60
Wall relative permittivity of dead yeast, ε_{wd}	60
Wall electrical conductivity of live yeast, σ_{wl}	0.014 S/m
Wall electrical conductivity of dead yeast, σ_{wd}	0.0015 S/m
Wall thickness of live yeast, t_{wl}	0.22 μm
Wall thickness of dead yeast, t_{wd}	0.25 μm
Membrane thickness of live yeast, t_{ml}	0.008 μm
Membrane thickness of dead yeast, t_{md}	0.008 μm

Table 2: Parameters used in the simulations.

Physics	Boundary condition	Discretization	Study
Creeping flow	Normal inflow velocity on inlets	P2 + P1	Stationary
	Zero static pressure on outlets		
	No-slip on channel walls		
Electric currents	Electric potential for electrodes	Lagrange Quadratic	Stationary (frequency domain)
	Electric insulation on the other channel boundaries		
Particle tracing for fluid flow	Release cells with random position from inlet I1	Formulation Newtonian	Time dependent
	Freeze on the channel walls		

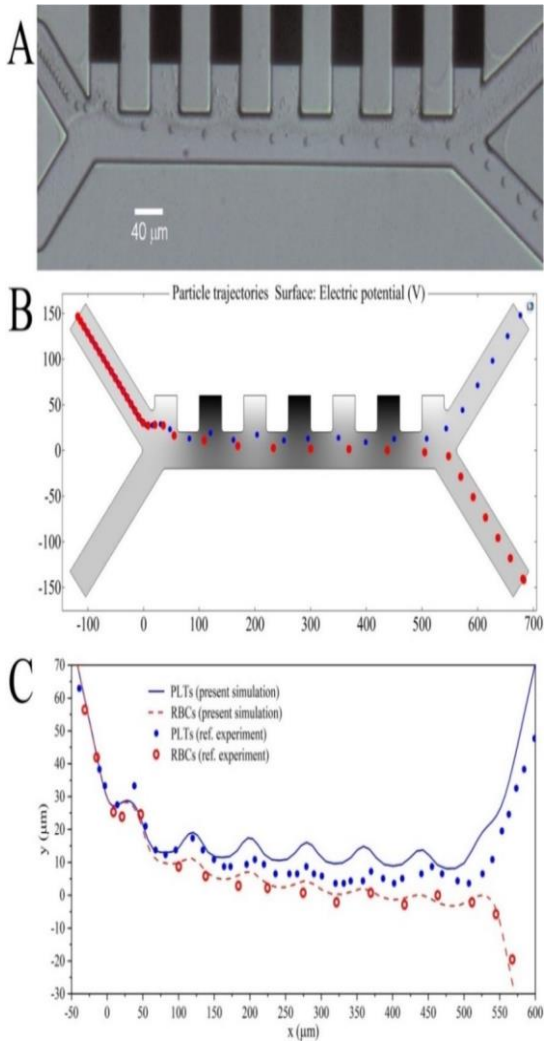

Fig. 3: Validation of numerical method with experimental data reported by Piacentini et al. [19].

trajectory of the cells obtained from the experimental and present numerical simulations, respectively, indicating qualitative agreement between the results. The lateral location of the cells along the microchannel (Fig. 3C)shows that the difference between the numerical results achieved from the present simulations and the experimental results reported by *Piacentini et al*. [19] is reasonable.

GRID STUDY

Choosing the appropriate grid is one of the most important steps in numerical simulations. A computational grid with few elements reduces the accuracy of the results and too many elements increase the computational time. Table 3 shows the maximum velocity and electric field norm obtained for different grid resolutions. The sample and buffer velocities are 60 μm/s and 360 μm/s, respectively. Besides, the applied voltage and frequency of the field are 4.35 V and 3.18 MHz, respectively. Also, the length of the electrodes is 60 μm and their distance from each other is 140 μm. Table 3 shows that the maximum values of fluid velocity and electric field norm achieved for grids with the number of elements greater than 34276 do not change and therefore this grid is selected for further simulations (Figure 4).

RESULTS AND DISCUSSION

Flow field

First, the velocity field is solved for different values of inlet velocity of sample flow (u_{Sample}) and buffer flow (u_{Buffer}) and the results are shown in Fig. 5. Fig. 5A depicts the velocity distribution when u_{Buffer} = 6 u_{Sample} and Fig. 5B demonstrates the velocity profile for u_{Sample} = 60 μm⁄s and different values of u_{Buffer}. As expected, the velocity profile is parabolic and the maximum velocity occurs on the channel centerline. Fig. 6 shows the velocity contours for u_{Sample} = 60 μm⁄s and u_{Buffer} = 360 μm⁄s. As can be seen, the velocity reaches zero on the microchannel walls due to the no-slip boundary condition.

Electric field

The distribution of electric field intensity (E) within the microchannel is shown in Fig. 7 when the electric potential applied to the electrodes is V_e = 4.35 V and the frequency is 3.18 MHz. It is found that the density of electric field lines is higher in the areas near the electrodes, indicating that the electric field is stronger in these areas. The arrows shown in Fig. 7 represent the direction of the field lines from the areas with the highest electrical potential (positive electrodes) to the areas with the lowest electrical potential (negative electrodes). Fig. 8 illustrates the impact of the voltage applied to the electrodes on the electric field norm. In this figure, the electric field intensity is plotted on the microchannel centerline. As can be seen, as the electric potential applied to the electrodes enhances, the electric field intensity is intensified.

Table 3: Grid-independence results.

Number of elements	Maximum velocity ($\times 10^{-4}$ m/s)	Maximum electric field norm (kV/m)
4188	7.159	26.400
5322	7.212	26.290
8128	7.253	26.286
14192	7.308	26.320
34276	7.334	26.165
38422	7.334	26.165
53162	7.334	26.165

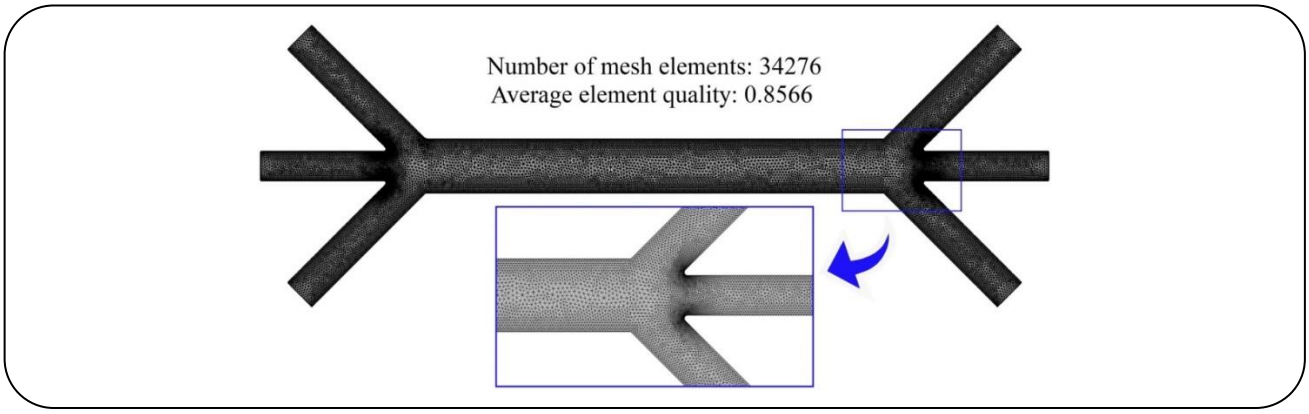

Fig. 4: Schematic of the grid used for the simulations.

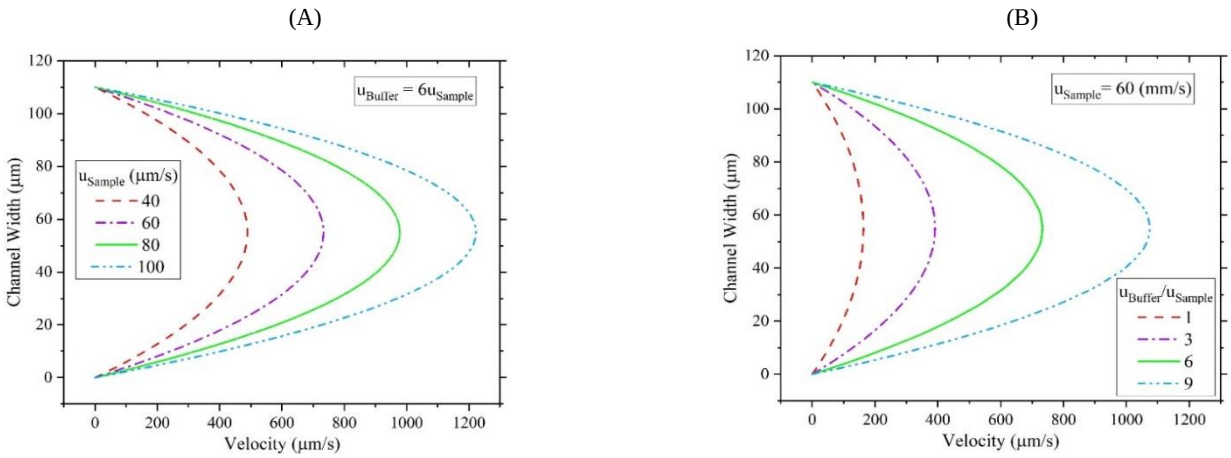

Fig. 5: Velocity profiles within the microchannel for (A) different values of u_{Sample} when $u_{Buffer} = 6\ u_{Sample}$ (B) u_{Sample} = 60 μm/s and different values of u_{Buffer}.

Effect of voltage

It is possible to calculate the trajectory of cells by solving the fluid velocity field and the electric field applied within the microchannel. Fig. 9 shows the trajectory of live (red) and dead (blue) yeast cells for different amounts of the voltage applied to the electrodes. In this part of the simulations, u_{Sample} = 60 μm/s, u_{Buffer} = 360 μm/s, l_e = 60 μm, d_e = 140 μm, and f = 3.18 MHz.

When V_e = ±2.35 V, live and dead yeast cells do not separate from each other and both pass through the outlet O2.

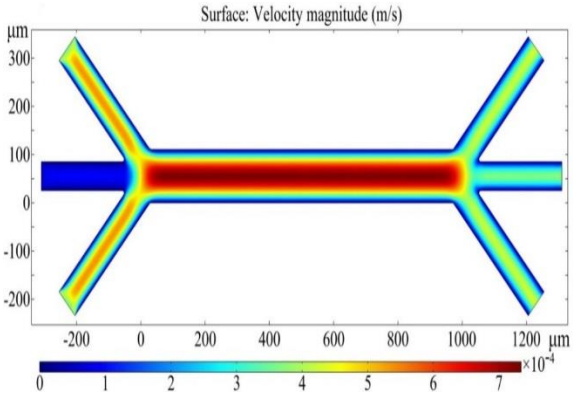

Fig. 6. Velocity contours within the microchannel for u_{Sample} = 60 μm/s and u_{Buffer} = 360 μm/s.

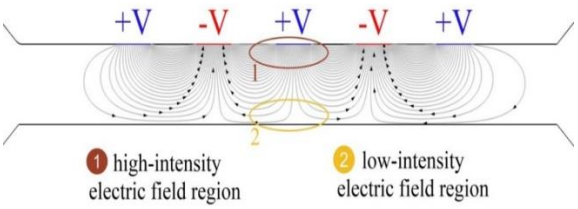

Fig. 7: Distribution of electric field intensity (E) within the microchannel when V_e = 4.35 V and f = 3.18 MHz.

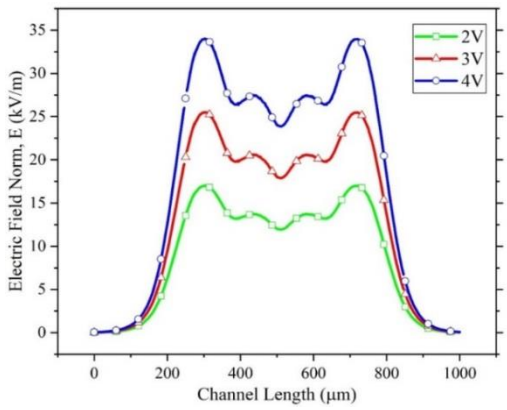

Fig. 8: Distribution of electric field intensity (E) on the microchannel centerline for different amounts of the electrical potential applied to the electrodes when f = 3.18 MHz.

In this case, the drag force F_{drag} prevails over the dielectrophoretic force F_{DEP} and cell separation is not observed. As the voltage applied to the electrodes increases and as a result, the electric field intensity gradient (∇E) is enhanced, the DEP force is intensified (Eq. (8)), leading to the dielectrophoretic motion of live yeast cells towards the areas near the electrodes (areas with higher electric field norm) and the isolation of live and dead cells. For V_e = ±4 V, the value of F_{DEP} is high enough to overcome F_{drag} and the live cells completely migrate towards outlet O1. Therefore, complete isolation of live and dead yeast cells occurs when V_e = 4 V. At this voltage, live yeast cells experience pDEP force and dead yeast cells experience nDEP force. A further increase in voltage enhances the distance between the live and dead cells until V_e = 4.70 V, where the live cells adhere to the upper wall of the microchannel and are trapped. The separation efficiency (SE) of live and dead cells is defined as the number of cells exited from an outlet divided by the total number of target cells injected into the microchannel. The purity of separation (SP) is calculated as the ratio of the number of the target cells in an outlet to the total number of cells exited from that outlet. By counting the number of cells in the two outlets, the efficiency and purity of cell separation can be determined in order to achieve the optimal conditions, i.e., the maximum separation efficiency and purity. The results for the simulated conditions of this section are presented in Fig. 10, showing that separation efficiency and purity are enhanced with the voltage until the cells are trapped. Also, the magnitudes of SE and SP are 100% when the applied electric potential is 4 and 4.35 V.

Effect of frequency

To assess the impact of applied frequency on the rate of cell separation, the simulations are carried out for u_{Sample} = 60 μm/s, u_{Buffer} = 360 μm/s, l_e = 60 μm, d_e = 140 μm, and V_e = 4.35 V. The trajectory of live and dead yeast cells is calculated and the results are shown in Fig. 11. When f = 3.18 Hz and 3.18 kHz, the live cells move towards outlet O3, indicating that the nDEP force is applied to the live yeast cells. Therefore, it can be expressed that the degree of polarization of live yeast cells is less than that of fluid at these frequencies and the polarization factor is negative (Eq. 9). By enhancing the frequency to 3.18 MHz, the live yeast cells migrate toward the outlet O1 and are affected by pDEP. Further increment of the frequency to 3.18 GHz causes live and dead cells to exit from the outlet O2. Under these conditions, F_{drag} prevails over F_{DEP} applied to the cells.

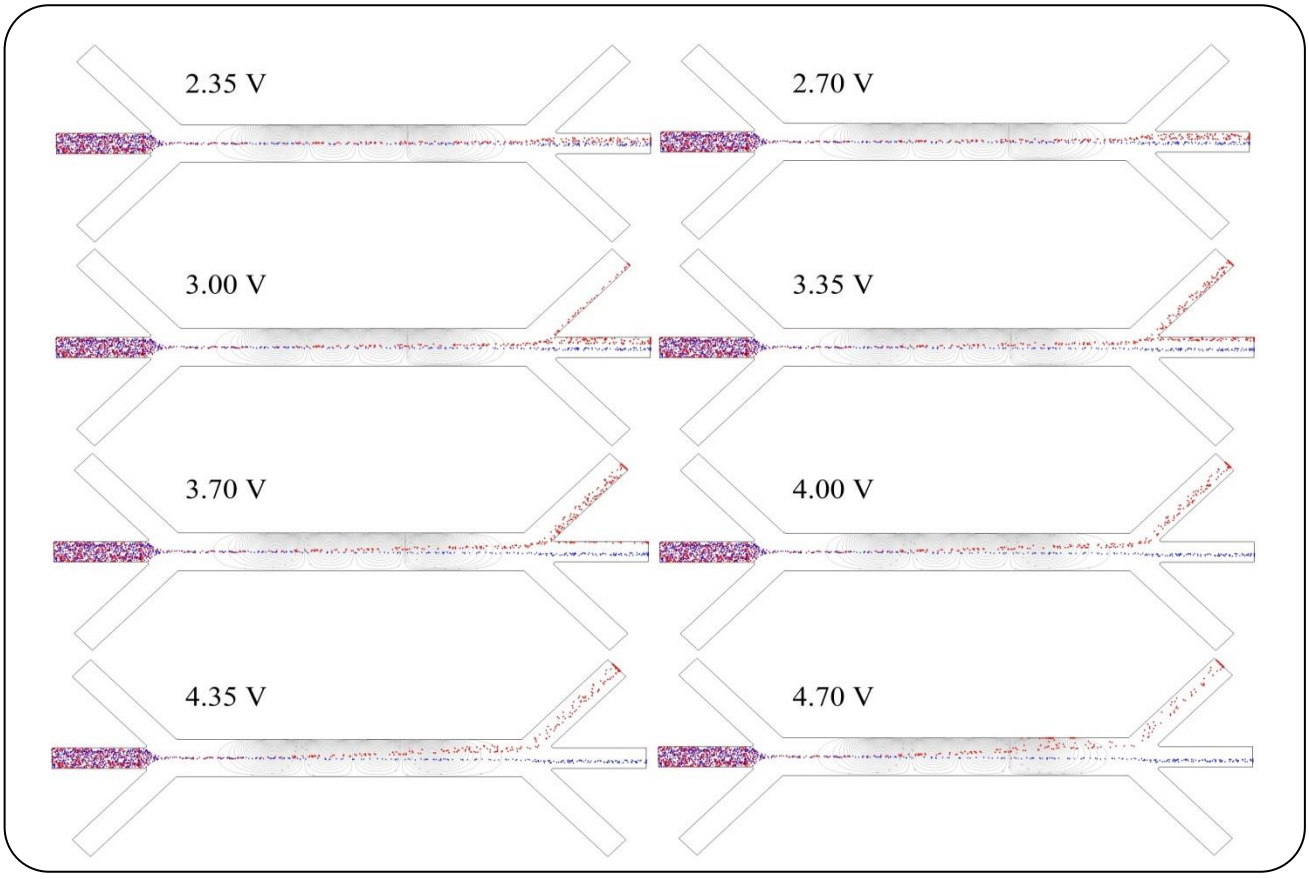

Fig. 9: Trajectory of cells for different amounts of the voltage applied to the electrodes.

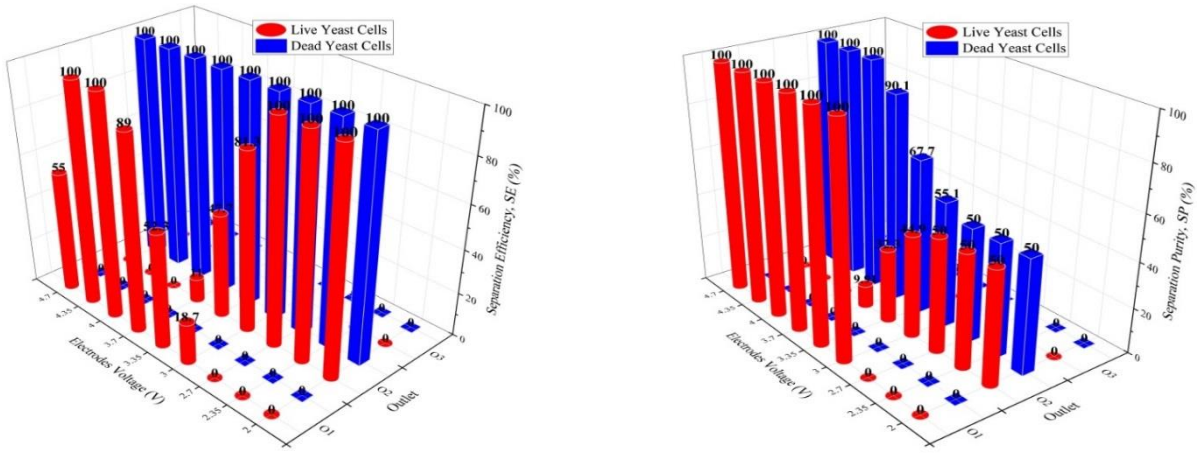

Fig. 10: Separation efficiency and purity for different amounts of the voltage applied to the electrodes.

Since live yeast cells withstand nDEP at 3.18 kHz and pDEP at f = 3.18 MHz, the transition from nDEP to pDEP takes place at a frequency between the values of 3.18 kHz and 3.18 MHz, which is known as the crossover frequency, in which $F_{DEP} = 0$. According to the experimental investigation of *Patel et al.* [1], the crossover frequency of live yeast cells is about 600 kHz. The magnitudes of SE and SP are presented in Fig. 12 for different frequencies. As observed in Fig. 11, SE = 100% can be achieved when f = 3.18 MHz.

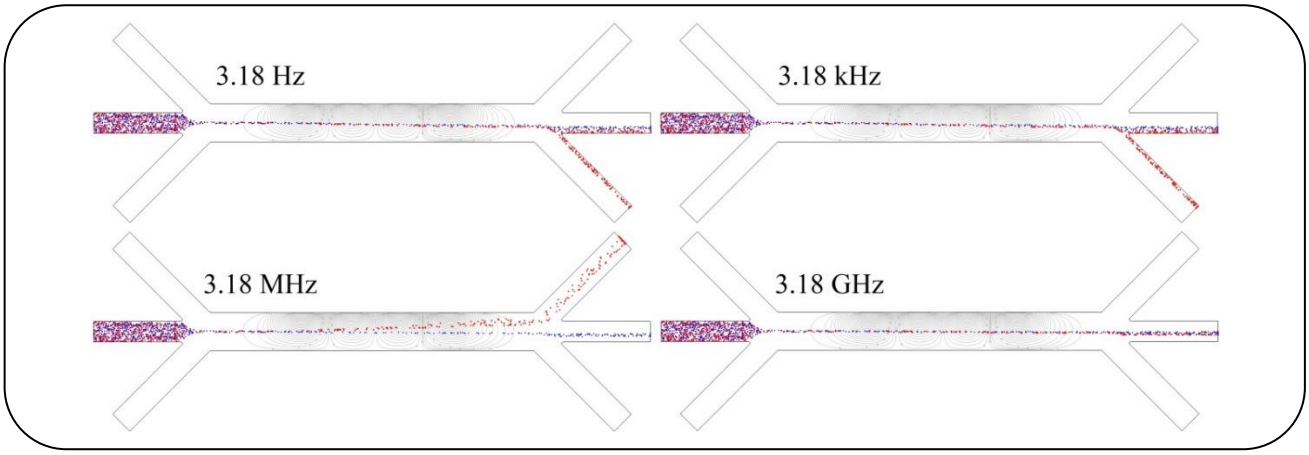

Fig. 11: Trajectory of cells for different values of electric field frequency.

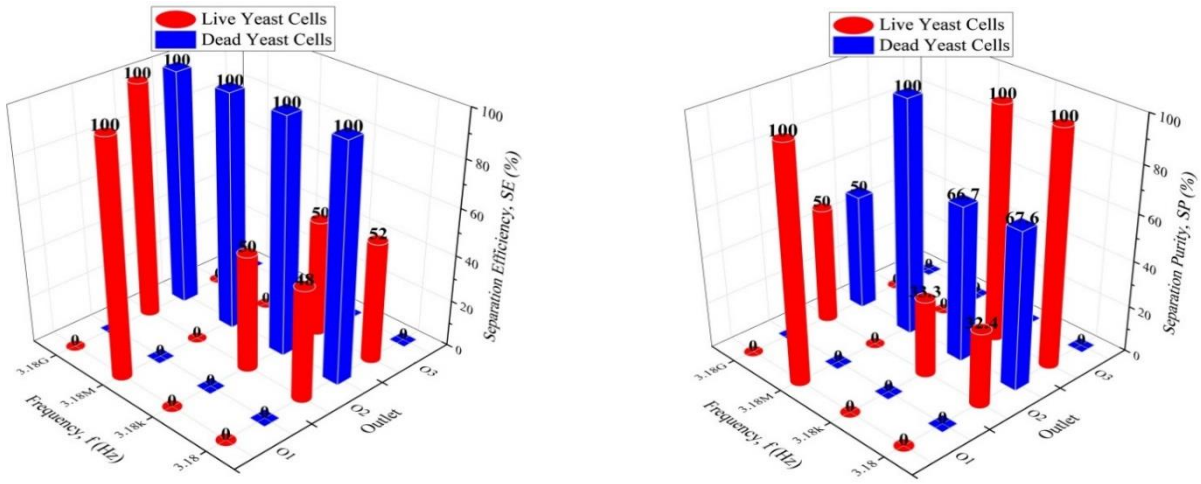

Fig. 12: Separation efficiency and purity for different values of electric field frequency.

Effect of electrode length

In this section, the effect of electrode length on cell separation is examined when u_{Sample} = 60 μm⁄s, u_{Buffer} = 360 μm⁄s, d_e = 140 μm, and V_e = 4.35 V. The trajectory of the cells is shown in Fig. 13. As can be seen, the separation rate increases with the length of the electrodes due to the expansion of areas with high electric field intensity toward the channel centerline, i.e. the initial location of yeast cells, and enhancing pDEP force on live yeast cells. It is observed that part of the live yeast cells is adhered to the upper wall of the microchannel and trapped when l_e = 80 μm. The quantitative amounts of SE and SP are presented in Fig. 14.

Effect of the distance between electrodes

To evaluate the influence of the distance between electrodes, it is assumed that u_{Sample} = 60 μm⁄s, u_{Buffer} = 360 μm⁄s, l_e = 60 μm, and V_e = 4.35 V. The trajectory of live and dead cells is plotted in Fig. 15. It is concluded that as the distance between the electrodes is reduced, the electric field norm increases and a strong pDEP force is applied to the live yeast cells. For d_e = 100 μm and 120 μm, a number of live cells adhere to the microchannel wall, as shown in Fig. 15. The values of separation efficiency and purity of cells are shown in Fig. 16, confirming that a reduction of d_e decreases SE and SP.

Effect of sample and buffer inlet velocity

In order to investigate the effect of sample inlet velocity on the separation rate, the following parameters are considered: $u_{Buffer} = 6\, u_{Sample}$, l_e = 60 μm, d_e = 140 μm, f = 3.18 MHz, and V_e = 4.35 V. The trajectory of live and dead cells is shown in Fig. 17. Increasing u_{Sample}

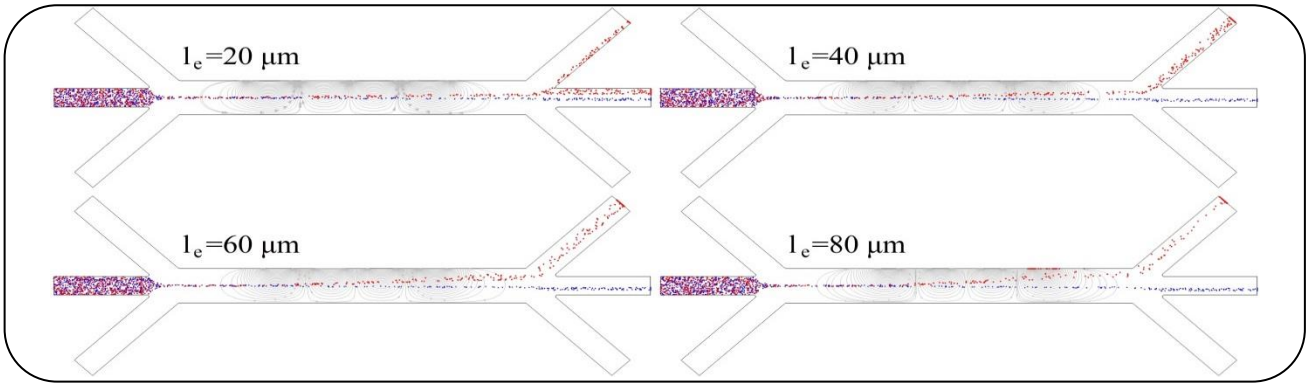

Fig. 13: Trajectory of cells for different values of the length of the electrodes.

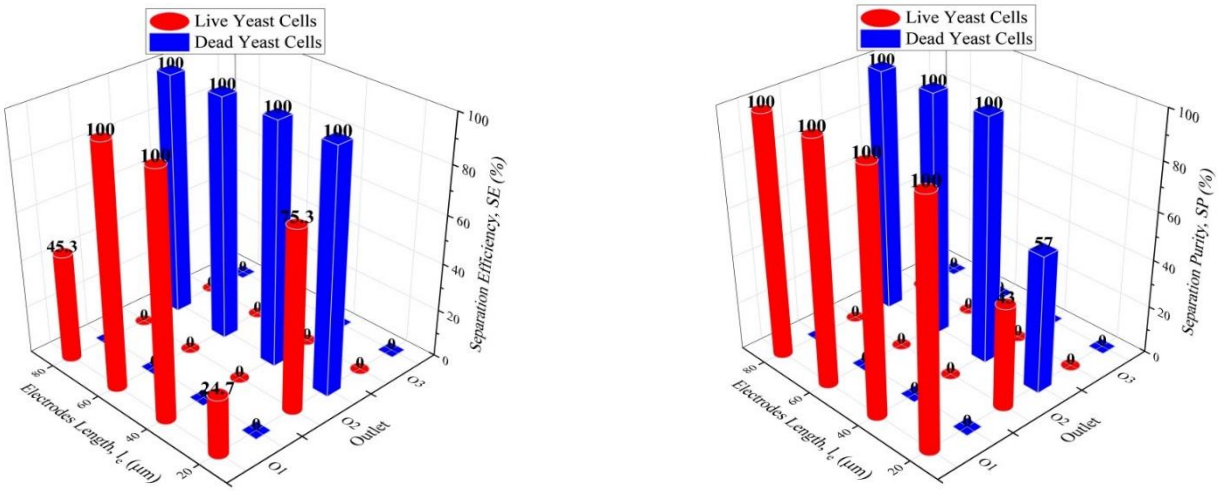

Fig. 14: Separation efficiency and purity for different values of electrode length.

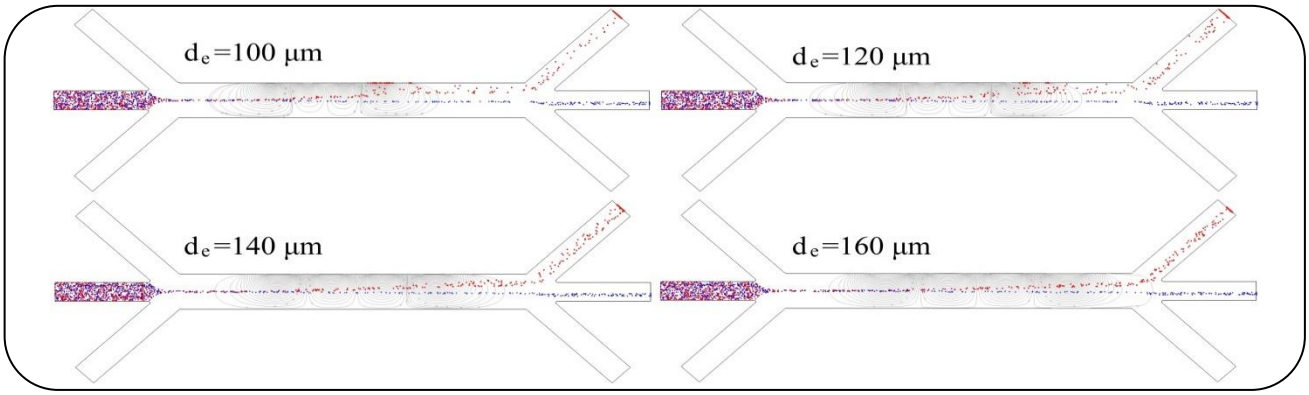

Fig. 15: Trajectory of cells for different values of the distance between the electrodes.

intensifies F_{drag} (Eq. 6) and vice versa. As the hydrodynamic force, i.e. F_{drag}, overcomes the dielectrophoretic force, the cells migrate towards the outlet O2. By reducing u_{Sample}, the pDEP force exerted on the live yeast cells overcomes the drag force and pushes them toward outlet O1. When u_{Sample} = 40 µm⁄s, the drag force is so small against the DEP force acting on the live yeast cells that all live yeast cells within the microchannel are trapped. The values of SE and SP are presented in Fig. 18.

The effect of buffer inlet velocity on SE and SP is investigated when u_{Sample} = 60 µm/s, l_e = 60 µm, d_e = 140 µm, f = 3.18 MHz, and V_e = 4.35 V. The trajectory of

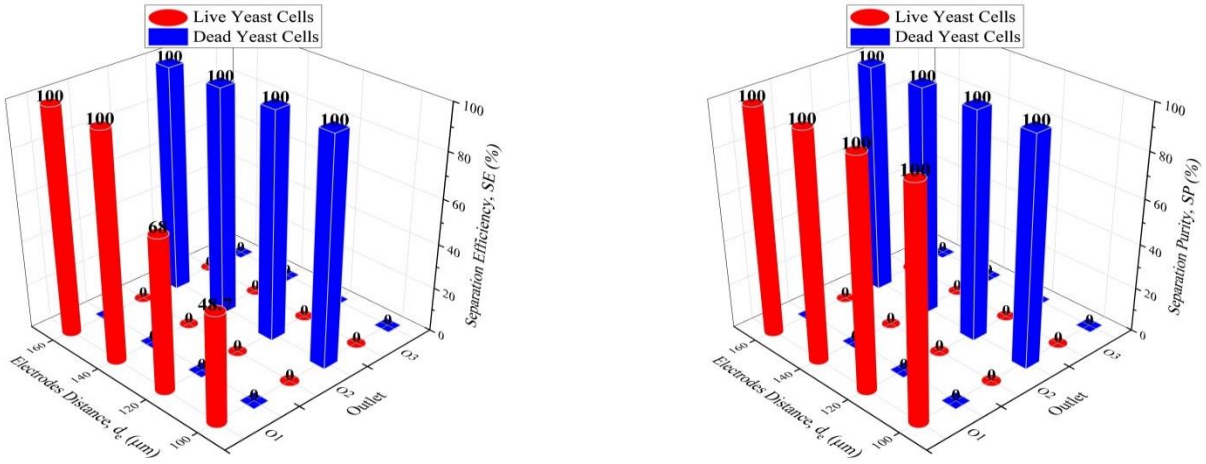

Fig. 16: Separation efficiency and purity for different values of the distance between the electrodes.

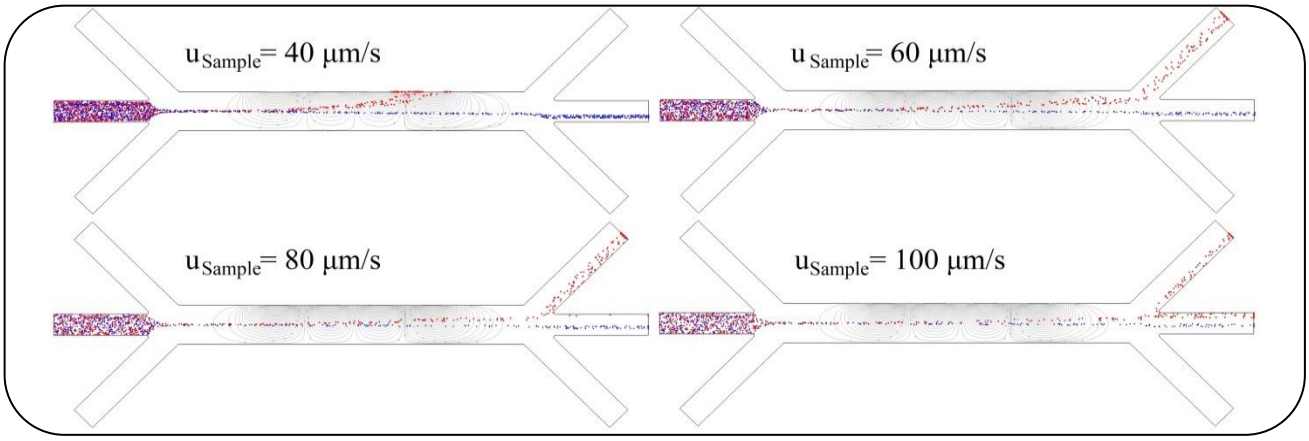

Fig. 17: Trajectory of cells for different values of sample inlet velocity.

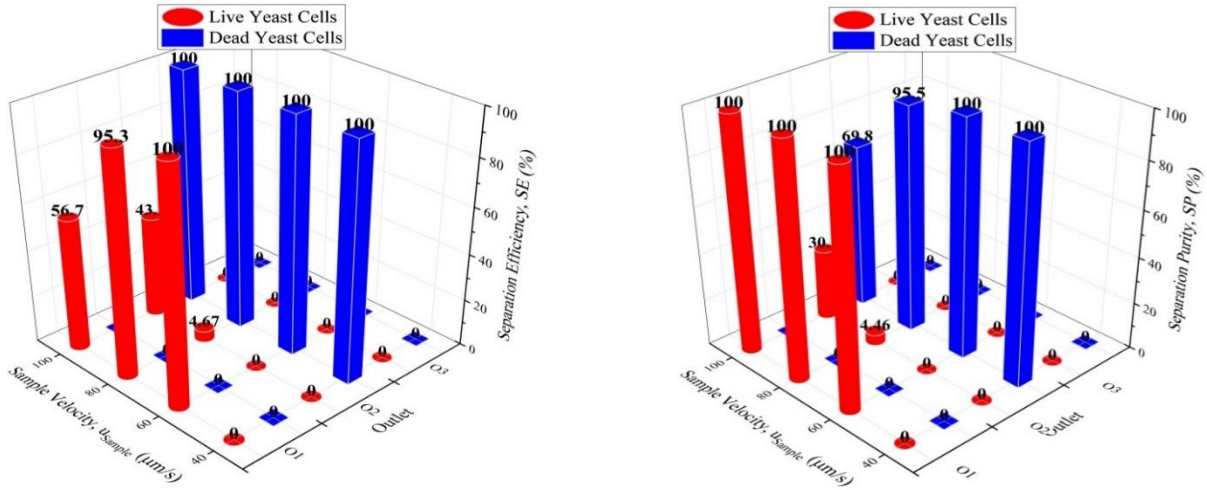

Fig. 18: Separation efficiency and purity for different values of sample inlet velocity.

Table 4: Optimal conditions for 100% cell isolation.

Parameter	Value
u_{Sample}	60 µm/s
u_{Buffer}	6 u_{Sample}
l_e	60 µm
d_e	140 µm
V_e	± 4.35 V
f	3.18 MHz

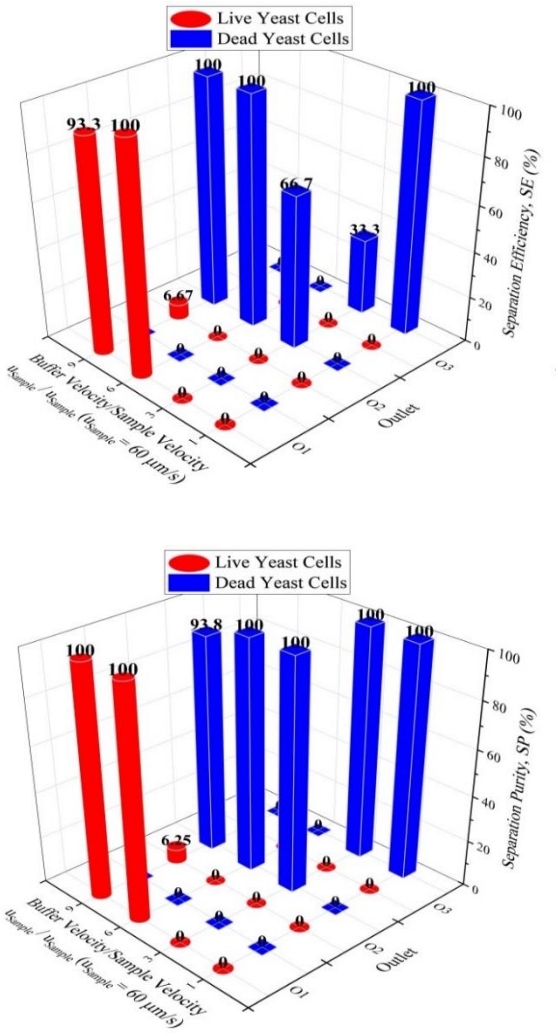

Fig. 19: Trajectory of cells for different values of buffer inlet velocity.

live and dead cells is shown in Fig. 19, indicating that the ratio of buffer velocity to sample one has a significant effect on cell separation. It is observed that complete separation of cells occurs when $u_{Buffer} = 6u_{Sample}$.

CONCLUSIONS

This study presents numerical isolation of live and dead yeast cells with different sizes, electrical conductivity, and permittivity using eDEP by employing COMSOL Multiphysics 5.6 software. The effect of various parameters, including electric potential, frequency, length of electrodes and their distance from each other, sample inlet velocity, and buffer inlet velocity on cell separation rate is examined. It is demonstrated that as the voltage applied to the electrodes is enhanced, the electric field intensity gradient increases, and consequently pDEP force applied to live yeast cells is intensified, leading to an enhancement in separation efficiency. SE = 100% is achieved for the voltages of ±4 and ±4.35 V. Further increase in voltage leads to that live yeast cells being trapped within the microchannel. The results show that reducing the frequency from 3.18 MHz decreases the polarization of live yeast cells. At f = 3.18 MHz, complete separation of live and dead yeast cells is observed, i.e. SE = 100% and SP = 100%. Further increase of frequency reduces the polarization of live yeast cells and decreases the DEP force, reducing the efficiency and purity of separation. It is found that a reduction in the inlet velocity reduces the drag force and vice versa. Complete separation is obtained when u_{Sample} = 60 µm⁄s and $u_{Buffer} = 6\ u_{Sample}$. According to the obtained results, the optimal conditions for the complete separation of live and dead yeast cells are provided in Table 4. The optimal amounts of applied voltage and frequency obtained from the present simulations are smaller than those reported by *Doh et al.* [21]. Besides, the frequency and voltage utilized by Matbaechi Ettehad and Wenger [22] were about 20 V and 5 MHz to isolate live and dead yeast cells completely.

The advantages of the proposed device for practical applications include the complete separation of live and dead yeast cells, small applied voltage (± 4.35 V) to achieve complete cell separation, high electric field frequency (3.18 MHz) for reduction of electrochemical reactions, including the production of bubbles, as well as the lack of dielectrophoretic motion of cells due to the charge of the cell membrane by static electricity [5].

Received :Dec. 06, 2022 ; Accepted :May 01, 2023

REFERENCES

[1] Patel S., et al., Microfluidic Separation of Live and Dead Yeast Cells Using Reservoir-Based Dielectrophoresis, *Biomicrofluidics*, **6(3)**: 034102 (2012).

[2] Bayareh M., Active Cell Capturing for Organ-On-A-Chip Systems: A Review, *Biomedical Engineering*, **67(6)**: 443-459 (2022).

[3] Chen L., et al., Dielectrophoretic Separation of Particles Using Microfluidic Chip with Composite Three-Dimensional Electrode, *Micromachines*, **11(7)**: 700 (2020).

[4] Bayareh M., An updated Review on Particle Separation in Passive Microfluidic Devices, *Chemical Engineering and Processing-Process Intensification*, **153**: 107984 (2020).

[5] Adekanmbi E.O., Srivastava S.K., Dielectrophoretic Applications For Disease Diagnostics Using Lab-on-A-Chip Platforms, *Lab on a Chip*, **16(12)**: 2148-2167 (2016).

[6] Çağlayan Z., Demircan Yalçın Y., Külah H., A Prominent Cell Manipulation Technique in BioMEMS: Dielectrophoresis, Micromachines, **11(11)**: 990 (2020).

[7] Li M., et al., A Review of Microfabrication Techniques and Dielectrophoretic Microdevices for Particle Manipulation and Separation, *Journal of Physics D: Applied Physics*, **47(6)**: 063001 (2014).

[8] Ramirez-Murillo C.J., de los Santos-Ramirez J.M., Perez-Gonzalez V.H., Toward Low-Voltage Dielectrophoresis-Based Microfluidic Systems: A Review, *Electrophoresis*, **42(5)**: 565-587 (2021).

[9] Xing X., et al., Label-Free Enumeration of Colorectal Cancer Cells From Lymphocytes Performed at a High Cell-Loading Density by Using Interdigitated Ring-Array Microelectrodes, *Biosensors and Bioelectronics*, **61**: 434-442 (2014).

[10] Pommer M.S., et al., Dielectrophoretic Separation of Platelets From Diluted Whole Blood in Microfluidic Channels, *Electrophoresis*, **29(6)**: 1213-1218 (2008).

[11] Yang F., et al., Dielectrophoretic Separation of Colorectal Cancer Cells, *Biomicrofluidics*, **4(1)**: 013204 (2010).

[12] Nie X., et al., High-Throughput Dielectrophoretic Cell Sorting Assisted by Cell Sliding on Scalable Electrode Tracks Made of Conducting-PDMS, *Sensors and Actuators B: Chemical*, **327**: 128873 (2021).

[13] Shiriny A., Bayareh M., On Magnetophoretic Separation of Blood Cells Using Halbach Array of Magnets, *Meccanica*, **55(10)**: 1903-1916 (2020).

[14] Shiriny A., Bayareh M., Inertial Focusing of CTCs in a Novel Spiral Microchannel, *Chemical Engineering Science*, **229**: 116102 (2020).

[15] Shiriny A., Bayareh M., Nadooshan A.A., Combination of Inertial Focusing and Magnetoporetic Separation in a Novel Microdevice, *Korean Journal of Chemical Engineering*, **38(8)**: 1686-1702 (2021).

[16] Kumar C.L., et al., Computational Microfluidic Channel for Separation of Escherichia Coli from Blood-Cells, *CMC Comput. Mater. Contin*, **67**: 1369-1384 (2021).

[17] Kumar M., et al., A Novel Microfluidic Device with Tapered Sidewall Electrodes for Efficient Ternary Blood cells (WBCs, RBCs and PLTs) separation, *Measurement Science and Technology*, **32(11)**: 115106 (2021).

[18] Guan Y., et al., Dielectrophoresis Separation of Platelets Using a Novel Zigzag Microchannel, *Micromachines*, **11(10)**: 890 (2020).

[19] Piacentini N., et al., Separation Of Platelets from Other Blood Cells in Continuous-Flow by Dielectrophoresis Field-Flow-Fractionation, *Biomicrofluidics*, **5(3)**: 034122 (2011).

[20] Mohamed Yousuff C., et al., Output Channel Design for Collecting Closely-Spaced Particle Streams from Spiral Inertial Separation Devices, *AIP Advances*, **7(8)**: 085004 (2017).

[21] Doh I. Cho Y.-H., A Continuous Cell Separation Chip Using Hydrodynamic Dielectrophoresis (DEP) Process, *Sensors and Actuators A: Physical*, **121(1)**: 59-65 (2005).

[22] Matbaechi Ettehad H., Wenger C., Characterization and Separation of Live and Dead Yeast Cells Using CMOS-Based DEP Microfluidics, *Micromachines*, **12(3)**: 270 (2021).

[23] Park K., Kabiri S., Sonkusale S., Dielectrophoretic Lb-on-CMOS Platform for Trapping and Manipulation of Cells, *Biomedical Microdevices*, **18(1)**: 6 (2016).

[24] Lyu C., et al., Simultaneous Electroporation and Dielectrophoresis in Non-Electrolytic Micro/Nano-Electroporation, *Scientific Reports*, **8(1)**: 1-13 (2018).